REGISTRATION AND FEATURE EXTRACTION FROM TERRESTRIAL LASER SCANNER POINT CLOUDS FOR AEROSPACE MANUFACTURING

Kate Pexman*, Stuart Robson

Department of Civil, Environmental and Geomatic Engineering, University College London
Gower Street, London WC1E 6BT, U.K. katherine.pexman.21@ucl.ac.uk, s.robson@ucl.ac.uk

Technical Commission II

KEY WORDS: Aerospace manufacturing, terrestrial laser scanning, registration, feature extraction, drilling, geometric primitives, spherical targeting, point clouds, laser tracking, Industry 4.0.

ABSTRACT:
Aircraft wing manufacture is becoming increasingly digitalised. For example, it is becoming possible to produce on-line digital representations of individual structural elements, components and tools as they are deployed during assembly processes. When it comes to monitoring a manufacturing environment, imaging systems can be used to track objects as they move about the workspace, comparing actual positions, alignments, and spatial relationships with the digital representation of the manufacturing process. Active imaging systems such as laser scanners and laser trackers can capture measurements within the manufacturing environment, which can be used to deduce information about both the overall stage of manufacture and progress of individual tasks. This paper is concerned with the in-line extraction of spatial information such as the location and orientation of drilling templates which are used with hand drilling tools to ensure drilled holes are accurately located. In this work, a construction grade terrestrial laser scanner, the Leica RTC360, is used to capture an example aircraft wing section in mid-assembly from several scan locations. Point cloud registration uses 1.5” white matte spherical targets that are interchangeable with the SMR targets used by the Leica AT960 MR laser tracker, ensuring that scans are connected to an established metrology control network used to define the coordinate space. Point cloud registration was achieved to sub-millimetre accuracy when compared to the laser tracker network. The location of drilling templates on the surface of the wing skin are automatically extracted from the captured and registered point clouds. When compared to laser tracker referenced hole centres, laser scanner drilling template holes agree to within 0.2mm.

1. INTRODUCTION

In an increasingly digital world, improving the level of automation in manufacturing is a requirement for forward progress, particularly for increased productivity. From aircraft to automobiles to mega-ships, large-scale multi-component assembly requires high levels of accuracy and precision, and can benefit from monitoring and modelling of the complex manufacturing processes. As components move and change through different stages of the manufacturing process, they accumulate variations. For a task such as aircraft manufacturing and assembly, components with miniscule variations combine to produce unique physical products, even if the products spawned from the same basic digital design model.

For multinational manufacturing corporations, the availability of a product-specific digital twin that is metrologically accurate, instrumental to the realization of Industry 4.0, is invaluable for both short-term and long-term monitoring and maintenance. The data required to create a digital twin, spanning both the temporal and spatial domains, can be captured using imaging technologies such as laser scanning and laser tracking. Live data from the factory floor can illustrate the real-time physical state of the product, and when matched back to the design data, can ease communication of product status and be used for quality assurance.

In order to track objects with an optical measurement system as they move around a physical environment, the objects to be tracked are most often equipped with recognizable targets that can be mapped into local coordinate frames or datums. From a productivity sense, it is inefficient to place targets on every component section that goes through an assembly line. A more efficient strategy would be to place targets on the jig structure supporting the component, such as an aircraft wing section, so that targets are independent of the manufactured object. This assumes a consistent relationship between the manufactured object and its supporting structure.

Currently, drilling templates, examples of which are shown in Figure 1, are manually affixed to the wing skin using pre-drilled alignment holes. The technique described herein explores capturing and modelling the drilling templates that are fixed to the aircraft wing surface to ensure that drill holes are made in the correct design locations. The process involves automatically and accurately locating individually shaped drilling templates placed in specified locations on the surface of an aircraft wing. Information as to correct placement and identification of the drilling templates is valuable as drilling, countersinking and fastening account for as much as 65% of the cost of aircraft assembly (Bullen 2013).

Figure 1: Example drilling templates

2. RELATED WORKS

2.1 Registration

Network design is an important consideration when planning a measurement survey that requires deployment of a network of sensors. Factors such as resolution, overlap, stand-off distance, incidence angle, and targeting must be considered, as well as optimizing the amount of data captured for the desired tasks. There has been significant work done on optimal network design in geodesy (Schmitt 1982) and photogrammetry (Fraser 1984) for example, but little when it comes to terrestrial laser scanning (TLS) for high precision surveys in manufacturing environments. A review of planning for scanning (P4S) using TLS in construction can be found in (Aryan, Bosché, and Tang 2021). An important piece of work was published by (Jia and Lichti 2019) regarding network design for scanning building interiors and exteriors with TLS. However, in most cases, TLS network planning is done empirically using the operator's prior experience and is largely dependent on the site or object of interest.

The main difference between laser scanning in buildings and laser scanning in a manufacturing space is that the former often requires 100% coverage (Scott, Roth, and Rivest 2003), whereas scanning for manufacturing tasks frequently needs to be a localized approach due to the required level of detail. In addition, the majority of work on TLS network design has considered surfaces typical in building facades (Lichti and Harvey 2002; Lichti 2005; Voegtle and Wakaluk 2009), rather than aerospace materials such as coated metals and composites.

2.1.1 Targeting: Artificial targets or features installed on or around an object can refine registration and unequivocally signalise locations and features of interest, versus the use of features such as edges, holes, or structure in the light reflected from the surface itself. However, marker installation is time consuming and, in most manufacturing cases, it is desirable to avoid the placement of targets directly on the manufactured piece. Targetless registration approaches rely heavily on the geometry and optical surface characteristics of the object being scanned, the strength of the observation network and the level of overlap between neighbouring scans. Alignment errors can arise during registration that then propagate into the measurements derived from the point cloud, especially when components have repeating features, a characteristic common in manufacturing.

Alternatively, targets can be used to strengthen the registration process, and can be used to reduce the level of overlap, and therefore the number of scans, required to represent an object. Yan Wang et al. (2021) determined that using a targeted approach increases the time spent before commencing the scanning process, however, it reduces both the time spent registering the scans together and the time spent collecting the scans as less overlap is required between the station set ups compared to a targetless approach.

For large, complex objects such as aircraft components, with varying levels of surface reflection due to varying surface finishes, the density of the captured points often varies greatly based on the proximity and imaging geometry of the object to the scanner. Aircraft wings are designed to aerodynamic requirements with a high level of smooth surface continuity. As a result, each wing cross section looks very similar to its neighbours, challenging a registration process that depends on identifying unique features, especially along a single axis, such as along the length of an aircraft wing.

Finally, it must be considered that not all metrology systems can make use of the same targets. The installation of targets becomes more complex and time-consuming if each measurement device in a network requires its own physical target type to be installed in the measurement environment. There are three main kinds of TLS targets: paper targets installed on flat surfaces, paddle targets installed on magnetic mounts or survey tripods, and spherical targets. Spherical targets are largely recognized as the most precise (Becerik-Gerber et al. 2011), with sphere fitting being used to precisely locate the targets within the point clouds. Becerik-Gerber et al. (2011) tested both a phase-based and a time-of-flight scanner, with both types performing best when dealing with spherical targets compared to checkerboard paper and paddle targets. However, none of the tests achieved sub-millimetre level registration errors likely due to the quality of the laser scanner and registration method. It is also worth considering the challenge of using paper targets because they cannot be viewed from oblique angles, unlike paddle and spherical targets which stick out from the surface to which they are affixed.

The technique of spherical target fitting from point clouds is built-in to most scanner and third-party point cloud registration software. It has also been widely researched with various changes to the general sphere fitting method, for example by adding fine registration to the process (Yun et al. 2015), dealing with occluded sphere edges (Yanmin Wang et al. 2014), the implementation of a modified RANSAC procedure (W. I. Liu 2019) and the use of geometrical constraints to find sphere centres (Franaszek, Cheok, and Witzgall 2009). Yang et al. (2021) investigated various registration errors and uncertainties that persist when using a laser scanner to measure gaps in aircraft wing assembly, concluding that the use of spherical targets can improve the efficiency of registration in PolyWorks.

2.2 Feature Extraction

Once registered, manually extracting information from point clouds is often time consuming, repetitive work that can be automated with algorithms involving pattern recognition and logic-based rules. Due to the nature of manufactured objects having regular shapes embedded within their design such as lines, planes and circles, pattern recognition techniques can be used to extract and model the shapes present within a point cloud to produce a 3D digital model of the physical object.

There has been a large amount of work done on the extraction and modelling of regular shapes from point clouds. Some of the most important developmental work in the extraction of regular shapes, referred to as geometric primitives, from point clouds first used range data (Roth and Levine 1993; Lozano-Perez, Grimson, and White 1987). Fitting shapes such as lines, planes and cylinders was further developed in (Taubin 1991; Lukács, Martin, and Marshall 1998). Since then, strategies have been widely used for a variety of shape-fitting tasks, adapting over time to accommodate increasingly growing point counts as laser scanning and computer processing technologies have advanced. A comprehensive review of segmentation strategies for point cloud feature extraction, (Grilli, Menna, and Remondino 2017), gives an overview of the state of the art in point cloud feature extraction. Currently, the task of point cloud feature extraction often uses machine learning or deep learning strategies, a review of which can be found in (W. Liu et al. 2019).

The holes in drilling templates are a special case of circle detection because they are actually very short cylinders. Some of the prevalent work in cylinder fitting includes (Chaperon and Goulette 2001; Rabbani and van den Heuvel 2005; Tran, Cao, and Laurendeau 2015; Nurunnabi et al. 2019). Generalized solutions for circle fitting are largely included as a first step in the 3D problem of cylinder fitting, where a 3D data set is sliced perpendicularly to the direction of the cylinders and circles are found within the 2D slice. Examples are given by (Nurunnabi et al. 2019), using Gaussian space to create a sphere (Chaperon and Goulette 2001; Tran, Cao, and Laurendeau 2015) or using a 2D Hough transform to extract cylinder parameters (Rabbani and van den Heuvel 2005). Additional circle-focused solutions include the extraction on non-overlapping ellipses (Maalek and Lichti 2021), and circle fitting in MLS datasets (Nurunnabi, Sadahiro, and Laefer 2018).

In previous work, holes have largely been treated as circles, as it simplifies the extraction problem into a 2D case. A small scale prototype solution was developed by (Rubio et al. 2017) which included a movable inspection cabin housing an optical measuring probe and imaging system to measure completed drill holes. A boundary point detection (BPD) method was developed in (Mineo, Pierce, and Summan 2018) based on the idea that a circle created using a boundary point (BP) and its two neighbours should not include any other points. The BP detector created by (Mineo, Pierce, and Summan 2018) was further refined by (Tang et al. 2022) who introduced a density-based threshold making the point-in-circle problem more robust to small outliers. They used their circle extraction algorithm to find tiny drill holes in an aircraft engine nacelle. However, their threshold was tuned to be dataset specific, and worked best only when dealing with a dataset of extremely high density (0.06mm between adjacent points).

3. METHODS

3.1 Registration

In this project, white matte 1.5” magnetized spherical scanning targets, (Figure 2), were placed in metrology nests located around a section of an aircraft wing section. Spheres were chosen as they are physically interchangeable with the 1.5” spherical mounted reflectors (SMRs) used by laser trackers in industrial manufacturing.

First, a Leica AT960MR laser tracker captured the SMRs in their magnetic metrology nests from multiple stations and computed their locations using a unified spatial metrology network (USMN) adjustment in New River Kinematics (NRK) Spatial Analyser (SA) software, version 2022.2.0624.8. The spherical scanner targets were then placed in the nests and a Leica RTC360 scanned the environment from multiple locations in high resolution (3mm at 10m). The RTC360 is a phase-based scanner with a laser wavelength of 1550 nm.

A built-in function in SA was used to automatically extract spheres from the point clouds. Given a sphere diameter, search tolerance, and minimum number of points found on the sphere, the SA algorithm can automatically find and extract spherical targets. The search tolerance is the maximum allowable deviation for a given point from the desired diameter in order to be considered a fit to the sphere (Spatial Analyzer 2021). The diameter of the spherical targets is 1.5” (38.1 mm), and the optimal values for the other parameters were experimentally determined to be a search tolerance of 0.3 mm and a minimum number of 50 points on the sphere surface. Alterations of these parameters either made the auto detect function find too many (false positives) or too few spheres in the point cloud. The centre of the extracted sphere is then automatically found using the ASTM E3125-17 (E57 Committee 2017) fitting algorithms on each extracted set of sphere points.

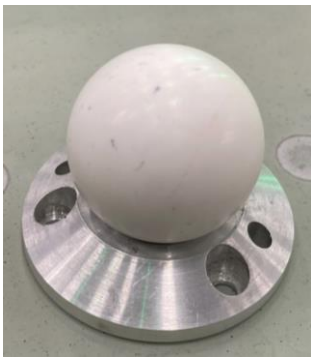

Figure 2: White spherical 1.5" laser scanner target sitting in magnetic nest

Point clouds output from each scanner location were then registered to the common coordinate system by performing a least squares best fit 7 parameter transformation with the laser tracker-measured target coordinates as the nominals. In the work presented here, the point clouds are registered into the coordinate frame set out by the laser tracker. The quality of the registration is evaluated by comparing the difference between the centre of the sphere measured using the laser tracker, and the centre of the sphere measured using the laser scanner.

3.2 Feature Extraction

The registered point clouds are used as the input dataset for an algorithm that automatically locates hole centres in a drilling template to identify if it has been placed within a specified tolerance. The algorithm works by extracting the close-to planar top surface of the drilling template and isolating it from the wing surface. This is done using a variation of RANSAC, originally developed by (Bolles and Fischler 1981; Fischler and Bolles 1981) and modified to include the use of M-estimators (MSAC) instead of a completely random selection of seed points (Torr and Zisserman 2000).

The algorithm uses a modification of the original BPD method developed by (Mineo, Pierce, and Summan 2018) based on the idea that a circle created using a BP and its two nearest neighbours should not include any other points. The BPD method was further refined by (Tang et al. 2022) who introduced a density-based threshold making the points-in-circle problem more robust to small outliers around the edge of a boundary, Figure 3. However, the threshold was tuned for extremely high-density simulated data, and therefore is not applicable to a construction grade laser scanner such as the RTC360, Figure 4. In addition, their work does not deal with holes in physical close proximity to each other. In the work presented here, the threshold is relaxed to work for a larger variation of point cloud densities.

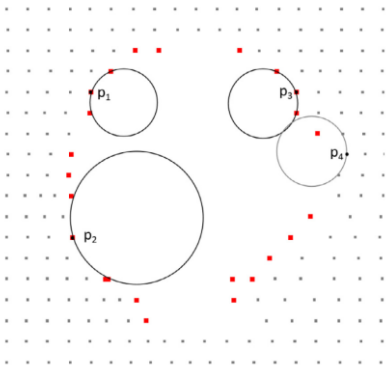

Figure 3: Boundary Point Detection, three holes create a circle (Tang et al. 2022)

In practice, the boundary points are detected by first computing the local resolution, β_i, around the seed point. This is done by computing the mean of the distances between the seed point and all of its neighbours, μ_i, and the standard deviation of those distances, σ_i (Equation 1).

$$\beta_i = \mu_i + 2\sigma_i \tag{1}$$

For every seed point, a circle is computed between it and every combination of two other points in its neighbourhood. The point is denoted as a potential boundary point if the radius of any created circle is larger than β_i. This is the original BPD method developed in (Mineo, Pierce, and Summan 2018), which does not deal with outliers found in scanning data close to the edge of a scanned object where each laser spot may contain systematic biases due to its footprint extending beyond the surface boundaries. As seen in p_4 in Figure 3, a boundary point may contain points within its created circle. In order to deal with such data, a boundary point inclusion threshold, n_{BPD}, is computed by comparing the number of points in the circle, c_{min}, to the total number of points in the neighbourhood, K (Equation 2).

$$n_{BPD} = 1 - \frac{c_{min}}{K} \tag{2}$$

The n_{BPD} value is computed for each boundary point, and potential boundary points are kept if the n_{BPD} value is larger than the threshold. The threshold value in (Tang et al. 2022) was experimentally derived to be 0.95 based on the point cloud resolution and the qualities of the scanned surface. The neighbourhood size is not given.

The BPD method is successful in extracting the boundary points of the drilling template (Figure 4). However, the method is very sensitive to a change in the n_{BPD} threshold value, with a higher threshold meaning less points are detected, while a lower threshold means more points are detected as boundary points. Figure 4 demonstrates that in data from the RTC360 scanning in high resolution, the threshold used by (Tang et al. 2022) does not detect enough BPs to determine the outline of the holes in the drilling template. The outline of the drill holes as well as the edges of the drilling template become clearer as the threshold is decreased, meaning more points are permitted within the created boundary circle.

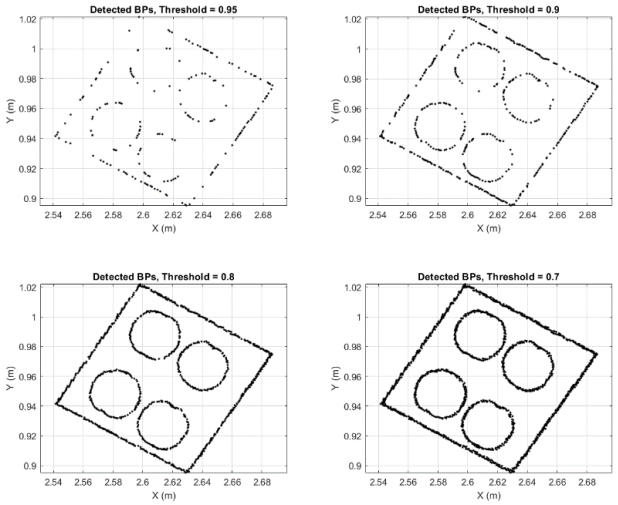

Figure 4: Boundary point differences for points-in-circle, n_{BPD}, threshold

Due to the inherent presence of outliers and gaps when using point clouds, particularly those captured by a construction grade terrestrial laser scanner, it an be hypothesized that the more boundary points extracted, the better the estimate of the circle centre will be, up to a breaking point. In this dataset, a threshold of 0.7 included sufficient BPs to form the complete outline of each template hole without gaps. The continuity of the detected boundary points is key, as they need to be clustered in order to estimate the centres of each individual hole. If gaps within the outline of the circle were kept to a minimum, i.e. by extracting more points, a complete outline of the holes could be obtained.

Once boundary points are identified, a connectivity analysis is performed to group points belonging to individual holes. In a validation step, estimated hole centres are compared to the reference hole centres measured by the laser tracker. The only prior information required is the hole diameter and the minimum separation between holes in the drilling template.

4. RESULTS AND ANALYSIS

4.1 Registration

Once the spheres are automatically extracted from the scans, the scans are registered to the network of control points as measured by the laser tracker. This is done using a 7 parameter best-fit transformation between the sphere centres. Each scan is individually registered to the control network, meaning each spherical target centre has slightly different coordinates. Analysis of output discrepancy vectors is that there is no discernible systematic error in the registration process between 0 and 1 mm; the registered target centres are equally spread in 3D around the target centre measured by the laser tracker. However, it is important to note that small discrepancies occur.

The quality of the sphere fit can be quantified by computing the 3D difference between the laser tracked and the laser scanned sphere centres for the same target after the best fit transformation has been performed. A simplified registration case is presented in Figure 5, where twelve repeated scans were captured of a linear set of targets; the instrument was not moved between scans.

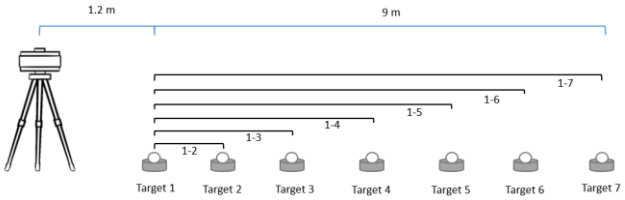

Figure 5: Scanning set up to test automatic extraction and quality of sphere fit

Sphere fit results are presented in Figure 6. Note that the number of spheres extracted from each scan varies, with targets closer to the scanner successfully extracted more often. Since each scan was matched independently, discrepancies between each tracked and scanned sphere centre are present. This variation is seen in Figure 6, where the spread of the difference is shown for each target. The larger the spread, the larger the variation in the difference between sphere centres in each scan.

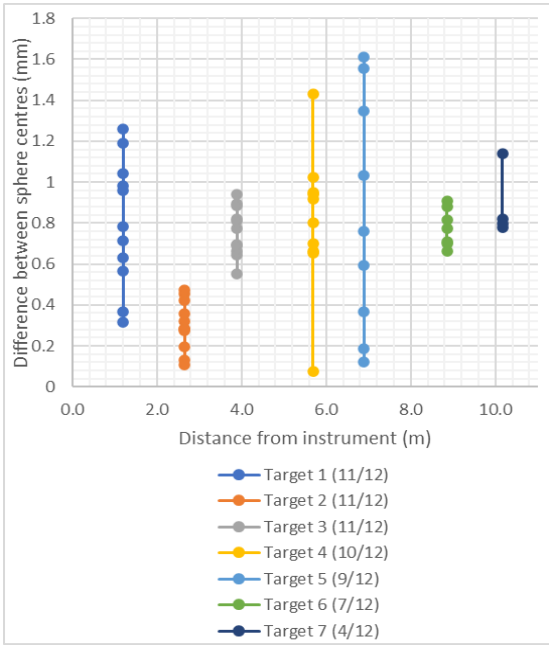

Figure 6: 3D difference between laser tracked sphere centre and laser scanned sphere centre vs. distance from instrument. Number of times each target was automatically detected from the scan is shown beside target number

The quality of the automated sphere extraction depends on both the difference between the centres of the laser scanned and laser tracked sphere, and the ability of the algorithm to automatically extract the spheres from the point cloud. Given the same fit tolerance and parameters, the number of targets extracted from the point cloud decreased as the distance from the instrument increased. This can be seen for Targets 6 and 7 in Figure 6, where only 7 and 4 spheres were extracted, respectively. The best fitting results are for Targets 2 and 3, located 2.7 m and 3.9 m from the instrument, respectively, and with 11/12 targets automatically extracted. The majority of the spherical targets were consistently extracted at ranges of 2 to 4 m, and the variation between laser tracked sphere centres and laser scanned sphere centres was consistently of the order of 0.4 mm.

The spread of the difference in sphere fit for Targets 4 and 5 is large, ranging from 0.1 mm to 1.6 mm. However, the distribution of the differences for Targets 4 and 5 do not follow the same pattern. The minimum and maximum difference for Target 4 could be outliers as without those two points, the distribution and mean would be very similar to the distribution and mean of Target 3. However, the sphere fit differences for Target 5 are evenly spread with no obvious outliers, meaning the sphere fit repeatability begins to degrade around 7 m. The steep inclination angle at Target 1 likely affected the distribution of the sphere fit differences of this closest point.

Due to variation in the distribution of the targets, the registration result differed for the experiments conducted. However, performing a best-fit adjustment with sub-millimetre RMS error was consistently achieved for scanning volumes up to 10 m^3.

4.2 Feature Extraction

The hole detection algorithm begins by using MSAC to extract a planar segment from the underlying wing skin (Figure 7).

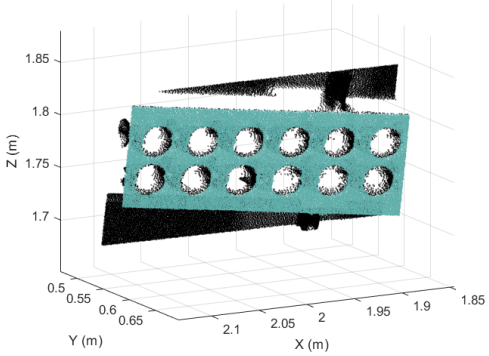

Figure 7: Planar segment (blue) detected from the point cloud (black), removes wing skin surface and interior of template holes

Boundary points are then extracted using the method described in Section 3.2. A linear model-driven MSAC is used to remove the linear edges of the drilling template. Next, a key step is to be able to separate the extracted boundary points into groups of points belonging to individual holes in the drilling template. This is vital to be able to compute the centres of each individual hole. The procedure is similar to region growing, in that points are clustered as long as the distance between points is smaller than a threshold value, in this case the minimum distance between holes in the template, 3 mm (Figure 8).

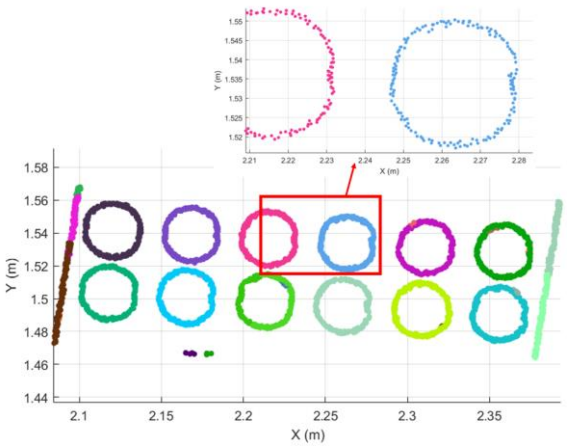

Figure 8: Points grouped by connectivity, pinching visible on either side of some drill holes

Finally, a circle is fit to each group of extracted points and a hole centre estimated. This hole centre can then be compared to

the hole centre measured by the laser tracker to validate the method (Figure 9 and Table 1).

The drilling templates were scanned from various ranges and incidence angles, in order to analyze the ideal orientation given the reflective nature of the sample brushed aluminum drilling template. Point cloud data were tested at their original resolution, and down sampled to 1 mm and 2 mm between points in the point cloud to evaluate the effect of density on the performance of the algorithm. Original point density was not consistent over the drilling template, but fluctuated around 0.3 mm on the section of the point cloud in question due to increasing distance of the template from the scanner location. The best performance of the algorithm in terms of minimizing the difference between the reference hole centres and the estimated hole centres was found to be from two scans at opposing oblique angles on either side of the drilling template, at a range of 2-3 m and incidence angle of 40-50˚, with a mean difference of 0.16 mm. The increase in incidence angle minimized the reflections from ambient lighting, improving the completeness of the point clouds compared to scans taken at minimal incidence angles. In addition, the scans were captured from approximately the same height as the template but from two opposing incidence angles, cancelling out the bias that appears when scanning short cylinders from high incidence angles.

Resolution (distance between points)	Original (~0.3mm[1])	1 mm	2 mm
Total Points	97795	38281	12114
Points in Plane	40536	15605	3930
BPs	3432	2159	899
Time (min)	13.1	2.9	0.5
Holes found	12/12	12/12	6/12
Mean difference (mm)	0.160	0.238	1.538
Delta x (mm)	0.035	-0.090	-0.734
Delta y (mm)	0.028	-0.006	-0.725

Table 1: Sample results from two combined oblique scans

[1] Approximate value, laser spot size is not given on manufacturer's technical sheet.

As seen in Table 1, the number of data points in the point cloud along with the number of points in the extracted plane and the number of boundary points detected reduces as the distance between points is increased. With a larger point cloud come longer processing speeds, but improvements in the mean difference between the reference hole centre and the hole centre estimated by the algorithm as well as the completeness of holes detected. Delta x and delta y values indicate the 2D direction of the difference between reference and estimated hole centres, in which an offset is present when using singular scans taken at oblique angles (Figure 9). The combination of the scans helps to reduce the directional offsets by increasing coverage, providing a complete representation of each template hole. It should be noted that scans from opposing incidence angles create a kind of self-compensation, and larger discrepancies would be expected from singular scans or from a wider distribution of drilling templates.

An example result from two scans is shown in Figure 9, where the reference (measured by the laser tracker) and estimated (from the point cloud captured by the laser scanner) hole centres and hole outlines are presented. The difference between the reference and estimated hole centres is quantified in Table 1 by the mean difference and delta x and y values. Additionally, the bias represented by the delta x and y values are presented in Figure 9, where the directional differences between reference and estimated hole centres have been multiplied by a factor of 50 for visualisation. It is clear from Figure 9 that the size of the difference vectors increases towards the right side of the drilling template, however, the direction of the difference vectors is not as consistent.

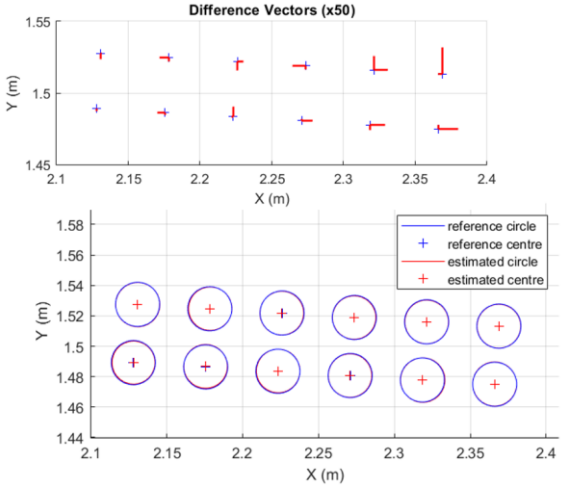

Figure 9: Circle centre discrepancies from two scans at opposing incidence angles; laser tracker reference in blue, laser scanner estimated in red

Despite the success of the hole detection algorithm, biased returns are prevalent when the scanner laser beam interacts with the inside of the template holes, seen in Figure 10 and Figure 11. The points captured inside the template hole do not describe the expected cylindrical shape. This is likely due to irregular reflections off the curved surface of the interior of the holes in the drilling template. When scanning from a high incidence angle, the incident laser bean can enter the hole, reflect off the interior wall, and continue downward rather than exiting the hole and returning to the scanner. Instead, the beam reflects multiple times until it hits either the bottom of the hole or some feature that reflects it back out again. This is sometimes referred to as optical 'rattle' and can cause path length extension.

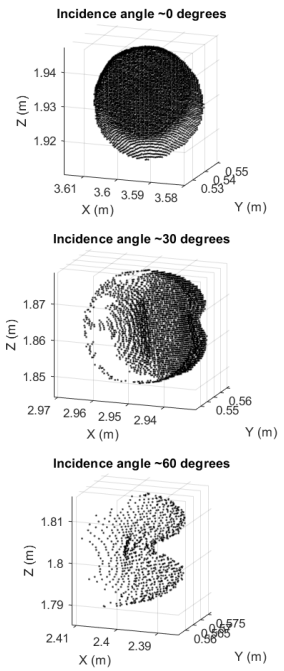

Figure 10: Hole signatures at various scan incidence angles

In addition to the curved shape, the brushed aluminium material likely impacted the returns from the drilling template. Figure 11 presents the surface of the drilling template (a) from which the holes were extracted in Table 1, as well as the returns from inside the holes in the template in Figure 11 (b), (c) and (d). These 'lobed' scan returns can be linked to the incidence angle of the scan location, as well as the optical rattle inside the scanned template holes. This is evident in Figure 11 (a) where 'pinching' can be seen on either side of the holes extracted in close proximity to the planar surface on the drilling template.

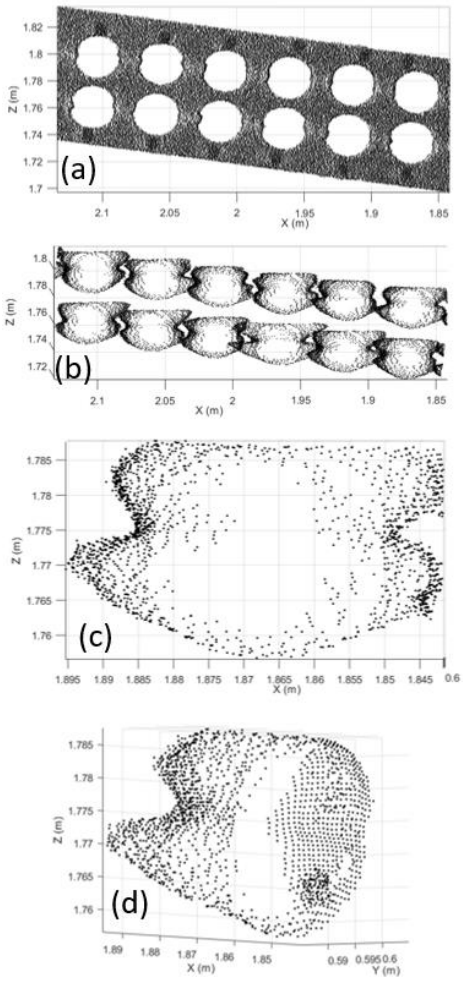

Figure 11: Biases shown in point cloud from two oblique angles; (a) planar surface of the drilling template, (b) returns from inside the drill holes with top surface removed, (c) and (d) plan and 3D view of the same singular drill hole.

Despite the systematic bias in the laser scanner measurements, the developed method was able to extract and compute the centres of the holes in the drilling template. Variations in scan range and incidence angle affected the result, however, the algorithm was consistently and reliably able to detect hole centres to the sub-millimetre level.

5. CONCLUSION

This work explored a precise registration method for point clouds captured by terrestrial laser scanners in manufacturing environments. Spherical targets were automatically extracted and used to register point clouds into a network of control points set out by a laser tracker and USMN adjustment. Once registered, these point clouds can be used to deduce valuable information on manufacturing progress and production. The registered point clouds were used to extract hole centres from drilling templates on the surface of an aircraft wing. Coverage, range and incidence angle have an impact on the quality of the captured scans. Manufacturing specifications and tolerances will determine the necessary scan setup and resolution.

Biased returns were recorded when scanning the drilling template from oblique incidence angles. These are likely due to the reflective nature of the aluminium interior surfaces of the drilling templates, as well as the depth and shape of the template holes. Additionally, it must be considered that template hole edges wear over time, and any deviation from circularity, even at the sub-millimetre level could affect the performance of the algorithm. Future work will include the exploration of optimal scanning angles, material properties of the drilling template and the use of scanners of differing metric capability.

REFERENCES

Aryan, Afrooz, Frédéric Bosché, and Pingbo Tang. 2021. "Planning for Terrestrial Laser Scanning in Construction: A Review." *Automation in Construction* 125 (May): 103551. https://doi.org/10.1016/j.autcon.2021.103551.

Becerik-Gerber, Burcin, Farrokh Jazizadeh, Geoffrey Kavulya, and Gulben Calis. 2011. "Assessment of Target Types and Layouts in 3D Laser Scanning for Registration Accuracy." *Automation in Construction* 20 (5): 649–58. https://doi.org/10.1016/j.autcon.2010.12.008.

Bolles, Robert C., and Martin A. Fischler. 1981. "A Ransac-Based Approach to Model Fitting and Its Application to Finding Cylinders in Range Data *." In , 637–43.

Bullen, George. 2013. *Automated/Mechanized Drilling and Countersinking of Airframes*. Pennsylvania, USA: SAE International.

Chaperon, Thomas, and Francois Goulette. 2001. "Extracting Cylinders in Full 3D Data Using a Random Sampling Method and the Gaussian Image." In *Vision Modeling and Visualization Conference 2001 (VMV-01)*. Stuttgart, Germany. https://hal.archives-ouvertes.fr/hal-01259641.

E57 Committee. 2017. "Standard Test Method for Evaluating the Point-to-Point Distance Measurement Performance of Spherical Coordinate 3D Imaging Systems in the Medium Range." ASTM International. https://doi.org/10.1520/E3125-17.

Fischler, M, and R Bolles. 1981. "Random Sample Consensus: A Paradigm for Model Fitting with Applications to Image Analysis and Automated Cartography." 1981. http://www.cs.ait.ac.th/~mdailey/cvreadings/Fischler-RANSAC.pdf.

Franaszek, Marek, Geraldine S. Cheok, and Christoph Witzgall. 2009. "Fast Automatic Registration of Range Images from 3D Imaging Systems Using Sphere Targets." *Automation in Construction* 18 (3): 265–74. https://doi.org/10.1016/j.autcon.2008.08.003.

Fraser, Clive S. 1984. "Network Design Considerations for Non-Topographic Photogrammetry." *Photogramm. Eng. Remote Sens*, 11.

Grilli, E., F. Menna, and F. Remondino. 2017. "A Review of Point Clouds Segmentation and Classification Algorithms." In *ISPRS - International Archives of the Photogrammetry, Remote Sensing and Spatial Information Sciences*, XLII-2-W3:339–44. Copernicus GmbH. https://doi.org/10.5194/isprs-archives-XLII-2-W3-339-2017.

Jia, Fengman, and Derek D. Lichti. 2019. "A Model-Based Design System for Terrestrial Laser Scanning Networks in Complex Sites." *Remote Sensing* 11 (15): 1749. https://doi.org/10.3390/rs11151749.

Lichti. 2005. "Spectral Filtering and Classification of Terrestrial Laser Scanner Point Clouds." *The Photogrammetric Record* 20 (111): 218–40. https://doi.org/10.1111/j.1477-9730.2005.00321.x.

Lichti, and Harvey. 2002. "The Effects of Reflecting Surface Material Properties on Time-of-Flight Laser Scanner Measurements." In . Ottawa, Canada.

Liu, Weiping, Jia Sun, Wanyi Li, Ting Hu, and Peng Wang. 2019. "Deep Learning on Point Clouds and Its Application: A Survey." *Sensors* 19 (19): 4188. https://doi.org/10.3390/s19194188.

Liu, W.I. 2019. "Novel Method for Sphere Target Detection and Center Estimation from Mobile Terrestrial Laser Scanner Data." *Measurement* 137 (April): 617–23. https://doi.org/10.1016/j.measurement.2019.02.025.

Lozano-Perez, T., W. Grimson, and S. White. 1987. "Finding Cylinders in Range Data." In *Proceedings. 1987 IEEE International Conference on Robotics and Automation*, 4:202–7. Raleigh, NC, USA: Institute of Electrical and Electronics Engineers. https://doi.org/10.1109/ROBOT.1987.1088007.

Lukács, Gabor, Ralph Martin, and Dave Marshall. 1998. "Faithful Least-Squares Fitting of Spheres, Cylinders, Cones and Tori for Reliable Segmentation." In *Computer Vision — ECCV'98*, edited by Hans Burkhardt and Bernd Neumann, 1406:671–86. Lecture Notes in Computer Science. Berlin, Heidelberg: Springer Berlin Heidelberg. https://doi.org/10.1007/BFb0055697.

Maalek, Reza, and Derek D. Lichti. 2021. "Robust Detection of Non-Overlapping Ellipses from Points with Applications to Circular Target Extraction in Images and Cylinder Detection in Point Clouds." *ISPRS Journal of Photogrammetry and Remote Sensing* 176 (June): 83–108. https://doi.org/10.1016/j.isprsjprs.2021.04.010.

Mineo, Carmelo, Stephen Gareth Pierce, and Rahul Summan. 2018. "Novel Algorithms for 3D Surface Point Cloud Boundary Detection and Edge Reconstruction." *Journal of Computational Design and Engineering* 6 (1): 81–91. https://doi.org/10.1016/j.jcde.2018.02.001.

Nurunnabi, Abdul, Yukio Sadahiro, and Debra F. Laefer. 2018. "Robust Statistical Approaches for Circle Fitting in Laser Scanning Three-Dimensional Point Cloud Data." *Pattern Recognition* 81 (September): 417–31. https://doi.org/10.1016/j.patcog.2018.04.010.

Nurunnabi, Abdul, Yukio Sadahiro, Roderik Lindenbergh, and David Belton. 2019. "Robust Cylinder Fitting in Laser Scanning Point Cloud Data." *Measurement* 138 (May): 632–51. https://doi.org/10.1016/j.measurement.2019.01.095.

Rabbani, Tahir, and Frank van den Heuvel. 2005. "Efficient Hough Transform for Automatic Detection of Cylinders in Point Clouds." *ISPRS WG III/3, III/4, V/3 Workshop "Laser Scanning 2005,"* September, 60–65.

Roth, Gerhard, and Martin Levine. 1993. "Extracting Geometric Primitives." *CVGIP: Image Understanding* 58 (1): 1–22.

Rubio, R., L. Granero, M. Sanz, J. García, and V. Micó. 2017. "Analysis and 3D Inspection System of Drill Holes in Aeronautical Surfaces." In , edited by Peter Lehmann, Wolfgang Osten, and Armando Albertazzi Gonçalves, 1032948. Munich, Germany. https://doi.org/10.1117/12.2270302.

Schmitt, Günter. 1982. "Optimization of Geodetic Networks." *Reviews of Geophysics* 20 (4): 877–84. https://doi.org/10.1029/RG020i004p00877.

Scott, William R., Gerhard Roth, and Jean-françois Rivest. 2003. "View Planning for Automated Three-Dimensional Object Reconstruction . . ."

Spatial Analyzer. 2021. "Spatial Analyzer User Manual." Hexagon Metrology, inc.

Tang, Hao, Laishui Zhou, Yuanpeng Liu, and Jun Wang. 2022. "Tiny Hole Inspection of Aircraft Engine Nacelle in 3D Point Cloud via Robust Statistical Fitting." *Measurement* 196 (June): 111250. https://doi.org/10.1016/j.measurement.2022.111250.

Taubin, G. 1991. "Estimation of Planar Curves, Surfaces, and Nonplanar Space Curves Defined by Implicit Equations with Applications to Edge and Range Image Segmentation." *IEEE Transactions on Pattern Analysis and Machine Intelligence* 13 (11): 1115–38. https://doi.org/10.1109/34.103273.

Torr, P.H.S., and A. Zisserman. 2000. "MLESAC: A New Robust Estimator with Application to Estimating Image Geometry." *Computer Vision and Image Understanding* 78 (1): 138–56. https://doi.org/10.1006/cviu.1999.0832.

Tran, Trung-Thien, Van-Toan Cao, and Denis Laurendeau. 2015. "Extraction of Cylinders and Estimation of Their Parameters from Point Clouds." *Computers & Graphics*, Shape Modeling International 2014, 46 (February): 345–57. https://doi.org/10.1016/j.cag.2014.09.027.

Voegtle, T, and S Wakaluk. 2009. "Effects on the Measurements of the Terrestrial Laser Scanner HDS 6000 (Leica) Caused by Different Object Materials." In . Paris, France: IAPRS.

Wang, Yan, Yuanpeng Liu, Qian Xie, Qiaoyun Wu, Xianglin Guo, Zhenghao Yu, and Jun Wang. 2021. "Density-Invariant Registration of Multiple Scans for Aircraft Measurement." *IEEE Transactions on Instrumentation and Measurement* 70: 1–15. https://doi.org/10.1109/TIM.2020.3016410.

Wang, Yanmin, Hongbin Shi, Yanyan Zhang, and Dongmei Zhang. 2014. "Automatic Registration of Laser Point Cloud Using Precisely Located Sphere Targets." *Journal of Applied Remote Sensing* 8 (1): 083588. https://doi.org/10.1117/1.JRS.8.083588.

Yang, Ye, Yan Jin, Mark Price, Gasser Abdelal, Colm Higgins, and Paul Maropoulos. 2021. "Investigation of Point Cloud Registration Uncertainty for Gap Measurement of Aircraft Wing Assembly." In *2021 IEEE 8th International Workshop on Metrology for AeroSpace (MetroAeroSpace)*, 164–69. https://doi.org/10.1109/MetroAeroSpace51421.2021.9511727.

Yun, Dongho, Sunghan Kim, Heeyoung Heo, and Kwang Hee Ko. 2015. "Automated Registration of Multi-View Point Clouds Using Sphere Targets." *Advanced Engineering Informatics* 29 (4): 930–39. https://doi.org/10.1016/j.aei.2015.09.008.